



## On the Dynamic Contact Angle in Capillary Flows

Mohammadmahdi Kamyabi\* , Ata Kamyabi

1. Department of Chemical Engineering, College of Engineering, Vali-e-Asr University of Rafsanjan, Rafsanjan, Iran. E-mail: mm.kamyabi@vru.ac.ir
2. Department of Chemical Engineering, College of Engineering, Shahid Bahonar University of Kerman, Kerman, Iran. kamyabi@uk.ac.ir

ARTICLE INFO	ABSTRACT
<p><b>Article History:</b> Received: 30 January 2021 Revised: 17 May 2021 Accepted: 18 May 2021</p> <p><b>Article type:</b> Research</p> <p><b>Keywords:</b> Capillary Number, Dynamic Contact Angle, Microfluidics, Static Contact Angle, Surface Tension</p>	<p>The displacement of the contact line (CL) between two arbitrary immiscible flowing fluids was modeled. The present model is valid for a wide range of viscosity ratios of the phases. The previously developed models reported in the literature were devoted to special cases, <i>i.e.</i>, high viscosity fluid pushing the low viscosity fluid. The present model reveals a direct relationship among the dynamic contact angle, the dimensionless pressure difference in the channel/tube, the Capillary numbers of both phases, and the characteristic length ratios of the channel/tube. The model was validated by agreeing with its predictions for the dynamic contact angle with the available data for a case of water-air flow inside a tube. Then, it was applied to more general cases with different viscosity ratios. According to the results, by increasing the ratio of the advancing phase's viscosity to the receding phase's viscosity, the dynamic contact angle reaches more quickly to its final value. It was also seen that by increasing the ratio of the length to the diameter of the tube the evolution of the dynamic contact, angle becomes slower. The most interesting point is that a unique behavior is seen and a master curve is achieved if the time becomes dimensionless with a changing parameter (not a fixed parameter). This facilitates the way to predict and interpret the dynamic contact angle in the most general way.</p>

## Introduction

Different fluids exhibit different behaviors in contact with solid surfaces. These differences are due to the difference in their willingness to wet the solid surface. This tendency is called fluid wetting or surface wettability. When two different immiscible (two phases) and static fluids are adjacent to the solid surface, the difference in their wettability results in a contact angle ( $\theta$ ), as shown in Fig. 1.

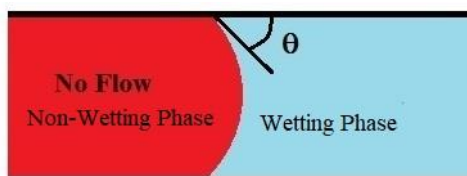


Fig. 1. The schematic of the contact line between two fluids and the observed contact angle

\* Corresponding Author: M.M. kamyabi (E-mail address: mm.kamyabi@vru.ac.ir)



When the two fluids are stationary, the observed contact angle is the static contact angle ( $\theta_s$ ). The static contact angle is well known and computable based on the Young-Laplace equation. The contact angle is again observed in the relative motion state of the phases and the solid surface. It is called the dynamic contact angle ( $\theta_d$ ) which its quantity is different from the static one depending on different factors [1]. In the relative motion mode of the phases, one phase moves forward, and the other is naturally pushed back. Hence, for each CL between the two phases, there will be two advancing and receding contact angles.

Many researchers have investigated the dynamic contact angle, most of which experimental studies [2-5]. These studies provide relations to predict the dynamic contact angle. However, as some of the most important ones will be shown below, they are only able to predict the dynamic contact angle in a limited range. Several studies concluded that the dynamic contact angle is dependent on some large-scale flow parameters such as the capillary number [6-8] and others believe that such a study should be conducted in the microscale by the use of molecular dynamics [9]. The difference between apparent and microscopic dynamic contacts was highlighted by Omori and Kajishima [10].

Hoffman [7] designed a device to measure the dynamic contact angle observed in a liquid-air flow passing through a capillary tube. He did it for several liquids and obtained the results for a relatively wide range of conditions, covering both viscous and inertial dominated regimes. This work showed that the advancing contact angle in the liquid-air flow is a function of the Capillary number and the static contact angle and a universal function. The well-known law of Hoffman-Tanner suggests that for a completely wetting fluid (*i.e.*, the static contact angle is approximately zero), the dynamic contact angle follows the relation of  $\theta_d^3 = 9Ca$  where  $Ca$  is the capillary number. This relationship holds for small contact angles [11]. Also, when the static contact angle is not zero, the well-known Hoffman-Vinoff-Tanner relation was found applicable as,  $\theta_d^3 - \theta_s^3 = 72Ca$  although its constant is in principle slightly dependent on the size of the flow system [12].

Jiang et al. [13] collected various available data for the dynamic contact angle and provided the Eq. 1 for predicting the dynamic contact angle for the viscous flow regime:

$$\frac{\cos \theta_s - \cos \theta_d}{\cos \theta_s + 1} = \tanh(4.96 Ca^{0.702}) \quad (1)$$

Bracke et al. [14] also obtained the Eq. 2 based on the results of a series of their own experiments:

$$\cos \theta_d = \cos \theta_s - 2(1 + \cos \theta_s)Ca^{1/2} \quad (2)$$

As it is clear, although many experimental studies were conducted to investigate the dynamic contact angle, no definitive and exact relationship has been derived yet from laboratory data that is true for all materials in all geometrical and physical conditions. Moreover, it has been shown that such relations are not applicable to predict the dynamic contact angle, especially at relatively high Capillary numbers [12,15]. All this adds up that laboratory measurements of dynamic contact angles are very difficult, especially at points very close to the CL.

Modeling is another way to study the dynamic contact angle. The major difficulty encountered in modeling the shape of the CL (and therefore the contact angle) is applying the no-slip wall boundary condition (which is a reasonable and widely used boundary condition for large-scale modeling) for such fluid-fluid-solid interface geometries which are very small in scale. This leads to the singularity in equations right at the CL, and consequently, the solution diverges [11, 16]. This issue was solved in different modeling works by supposing a slip in very

close distances of the CL, e.g., distances less than  $S$  [17, 18]. However, no convincing experiment or theory has yet been found to support or reject these kinds of methods [9].

Cox [17] developed an approximate method and assumed that in the distances less than  $S$  (slip length) the dynamic contact angle tends to the static contact angle, and finally reached to Eq. 3:

$$g(\theta_d, M) - g(\theta_s, M) = Ca [\ln(\varepsilon^{-1}) + Q] + O(Ca^2) \quad (3)$$

where  $\varepsilon=S/R$ ,  $Q$  depends on the slip model and imposed boundary condition,  $g$  is a simple function which tends to the Hoffman universal function as the viscosity ratio of the fluids tends to the infinity.

Eggers and Stone [11] showed the importance of the characteristic lengths in predicting the dynamic contact angle. They concluded that for the full wetted state (i.e., when  $\theta_s=0$ ), the dynamic contact angle at a distance of  $x$  from the CL is predicted with the Eq. 4:

$$\theta_d^3(x) = 9Ca \ln\left(\frac{x}{S} ca^\beta\right) \quad (4)$$

where  $\beta$  is a positive constant and depends on the type of the physical slip mechanism (such as Van der Waals, Navier slip, nonlinear slip, etc.), which is assumed to be applicable at the locations close to the CL (distances less than  $S$ ), although this relation provides a good physical view of the dynamic contact angle, it has a great deal of uncertainty due to how the  $\beta$  constant and the microscope length ( $S$ ) are taken into account.

Accurate prediction of most large-scale models is dependent large-scale models depend on some microscale parameters, such as slip length ( $S$ ). Hence, microscale (molecular) models were mostly dedicated to predicting the slip length. These models were also used to predicting the relationship of dynamic contact angle with flow velocity or Capillary number [19, 20]. They have also been developed in order to predict the effects of the uneven solid surfaces on the dynamic contact angle [21].

As it was seen, most studies on the dynamic contact angle considered the steady flow of a case of two-phase liquid-air. It means the viscosity of one phase was deliberately ignored in comparison with the other phase. However, by conducting experiments on the two-phase flows of different liquid-air and liquid-liquid systems, Fermigier and Jenffer [22] found that their results of dynamic contact angle for liquid-air systems are in good agreement with the well-known Hoffman-Tanner relation as well as Cox's theory predictions. Still, the data obtained for the dynamic contact angle in liquid-liquid systems was greater than predictions by existing theories. They noticed the influence of the viscosity ratio of the phases (i.e., the effect of the Capillary number of both phases) on the dynamic contact angle.

According to what is known so far, the effects of viscosity ratio and characteristic lengths on the dynamic contact angle should not be underestimated by the capillary number of only one phase. However, no definitive theoretical equation or comprehensive experimental relationship has yet been derived that encompasses all these parameters together. The current study tried to start the development of such a relation, although with some simplification assumptions at first. The model considers the two phases separately and starts with the famous Hagen-Poiseuille equation for the single-phase flows in tubes and the equivalent equation for the channels. This idea was first suggested by Washburn [23] and then widely used in a series of publications by Hilpert [24-27] where the liquid infiltration into and liquid withdrawal from capillary tubes was modeled. Using the Young-Laplace equation for predicting the contact angle as the function of pressure drop across the CL, the model was completed to obtain the final relation for the dynamic contact angle. Cai et al. [28, 29] also used the same idea for predicting spontaneous inhibition in capillaries. Although these studies examined different geometric and physical states in great detail, the viscosity of the second phase was ignored. They also assumed the pressure difference between the two ends of the capillary to be zero and used the experimental

models mentioned earlier to predict the dynamic contact angle. However, in the present study, this problem is tried to be investigated in its most general case of two-phase flow without mentioned limitations. The effects of the viscosity ratio and characteristic length ratio will be quantified for the first time.

## Theory

According to Fig. 2, it was assumed that the two fluids flow from left to right in a capillary channel and a capillary tube. The dynamic contact angle was defined as the contact angle between the wetting fluid (e.g., fluid 1) and the solid surface, as shown in this figure.  $P_1$ ,  $P_2$ ,  $P_3$ , and  $P_4$  were the pressures at the places shown in this figure.

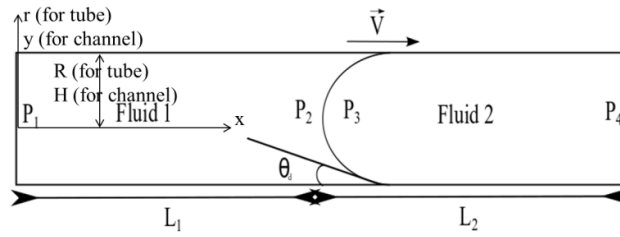


Fig. 2. The simplified geometries of the channel flow and the tube flow

To study the fluids flow in such conditions, the following assumptions were intended:

1. Fluids are immiscible, and fluid 1 (according to Fig. 1) is the wetting phase.
2. Fluids are Newtonian, and flows are incompressible (Because of low Mach number).
3. The surface tension between the fluids as well as between the fluid and the solid wall is constant.
4. The flows are laminar (*i.e.*, the dense regime is dominant due to low Reynolds numbers).
5. The pressure at each point of any cross-sectional area is constant and only changes along the channel/tube length.
6. The flows are fully developed, and the pressure changes linearly in each phase.
7. Gravity is neglected (Because the Bond number ( $Bo = \frac{(P_1 - P_4)gL^2}{\sigma}$ ) is low for such assumed microscale flows).
8. The interface moves at a constant velocity
9. Fluids flow from left to right at a quasi-steady-state condition.

Applying Navier-Stokes equations in the flow direction for each fluid, by considering the above assumptions, along with using mass conservation equation, the Eq. 5 and Eq. 6 are obtained:

$$\text{For channel flow: } \begin{cases} \text{for fluid 1: } \frac{P_1 - P_2}{L_1} + \mu_1 \frac{d^2 u_1}{dy^2} = 0 \\ \text{for fluid 2: } \frac{P_3 - P_4}{L_2} + \mu_2 \frac{d^2 u_2}{dy^2} = 0 \end{cases} \quad (5)$$

$$\text{For tube flow: } \begin{cases} \text{for fluid 1: } \frac{P_1 - P_2}{L_1} + \frac{\mu_1}{r} \frac{d}{dr} \left( r \frac{du_1}{dr} \right) = 0 \\ \text{for fluid 2: } \frac{P_3 - P_4}{L_2} + \frac{\mu_2}{r} \frac{d}{dr} \left( r \frac{du_2}{dr} \right) = 0 \end{cases} \quad (6)$$

Supposing that no-slip boundary condition is valid on the wall surfaces for both fluids, the solutions of Eqs. 5 and 6 are Eq. 7 and Eq. 8:

$$\text{For channel flow: } \begin{cases} P_1 - P_2 = \frac{3\bar{U}L_1\mu_1}{H^2} \\ P_3 - P_4 = \frac{3\bar{U}L_2\mu_2}{H^2} \end{cases} \quad (7)$$

$$\text{For tube flow: } \begin{cases} P_1 - P_2 = \frac{8\mu_1L_1\bar{U}}{R^2} \\ P_3 - P_4 = \frac{8\mu_2L_2\bar{U}}{R^2} \end{cases} \quad (8)$$

where  $\bar{U}$  is the average velocity of the fluids inside the tube/channel. Since the average velocity is the same for both fluids, it has no indexes. As expected, the obtained equation for the capillary tube flow is the popular equation of Hagen-Poiseuille.

Now, by applying force balance to the CL and using the Young-Laplace equation, Eq. 9 and Eq. 10 are obtained:

$$\text{For channel flow: } P_2 - P_3 = -\frac{\sigma \cos(\theta_d)}{H} \quad (9)$$

$$\text{For tube flow: } P_2 - P_3 = -\frac{2\sigma \cos(\theta_d)}{R} \quad (10)$$

By adding Eqs. 9 and 10 to Eqs. 7 and 8, respectively, the following Eqs. 11 and 12 are derived:

$$\text{For channel flow: } \cos(\theta_d) = \frac{3}{H} (Ca_2L_2 + Ca_1L_1) - \frac{(P_1-P_4)H}{\sigma} \quad (11)$$

$$\text{For tube flow: } \cos(\theta_d) = \frac{4}{R} (Ca_2L_2 + Ca_1L_1) - \frac{(P_1-P_4)R}{2\sigma} \quad (12)$$

where  $Ca_1 = \frac{\mu_1\bar{U}}{\sigma}$  and  $Ca_2 = \frac{\mu_2\bar{U}}{\sigma}$  mean the Capillary numbers based on the viscosities of fluids 1 and 2, respectively.

The terms  $\frac{(P_1-P_4)H}{\sigma}$  and  $\frac{(P_1-P_4)R}{2\sigma}$  can be assumed as the dimensionless pressure differences in the whole channel and the tube, respectively. Therefore, Eqs. 11 and 12 show an explicit relationship among the dynamic contact angle observed in the channel/tube, the dimensionless pressure differences between the two sides of the channel/tube, the Capillary numbers of both phases and the characteristic lengths of the channel/tube. Eqs. 11 and 12 are the main ones and all the following relations developed for the dynamic contact angle are based on these two equations.

As a simpler case, the length of the channel/tube ( $L_1+L_2$ ) can be assumed long. Therefore, it can be assumed that  $L_1=L_2 \cong L$  is not changed notably at short time intervals. Therefore, Eqs. 11 and 12 convert to the Eqs. 13 and 14 as:

$$\text{For channel flow: } \cos(\theta_d) = \frac{3L}{H} (Ca_2 + Ca_1) - \frac{(P_1-P_4)H}{\sigma} \quad (13)$$

$$\text{For tube flow: } \cos(\theta_d) = \frac{4L}{R} (Ca_2 + Ca_1) - \frac{(P_1-P_4)R}{2\sigma} \quad (14)$$

Eqs. 13 and 14 are valid at the conditions where steady assumption is not far from reality. However, these equations demonstrate the effect of the ratio of the characteristic lengths (vividly  $L/H$  for the channel and  $L/R$  for the tube) on the dynamic contact angle.

However, in transient conditions, as the fluids flow through the channel/tube, the lengths of  $L_1$  and  $L_2$  change so that at a certain time of  $t$  from the beginning of the flow,  $L_1 = L_{1,0} + \bar{U}t$  and  $L_2 = L_{2,0} - \bar{U}t$  where  $L_{1,0}$  and  $L_{2,0}$  are the initial values of  $L_1$  and  $L_2$  respectively. Therefore, Eqs. 11 and 12 convert to the Eqs. 15 and 16, respectively:

$$\text{For channel flow: } \cos(\theta_d) = \frac{3}{H} [Ca_2(L_{2,0} - \bar{U}t) + Ca_1(L_{1,0} + \bar{U}t)] - \frac{(P_1-P_4)H}{\sigma} \quad (15)$$

$$\text{For tube flow: } \cos(\theta_d) = \frac{4}{R} [Ca_2(L_{2,0} - \bar{U}t) + Ca_1(L_{1,0} + \bar{U}t)] - \frac{(P_1 - P_4)R}{2\sigma} \quad (16)$$

Using weather Eqs. 13 and 14 or Eqs. 15 and 16 depends on the real test conditions (steady or transient), which one may apply in the laboratory to obtain data. However, we continue with the Eqs. 13 and 14 hereafters, although all following equations can also be re-derived for Eqs. 15 and 16.

It is expected that the fluids do not flow for a certain value of pressure difference between the two ends of the channel/tube (e.g., for  $P_4 - P_1 = P_3 - P_2 = \Delta P_{st-lr}$ ). For the pressure differences ( $P_4 - P_1$ ) less than  $\Delta P_{st-lr}$  the fluids flow from left to the right, and for the pressure differences higher than  $\Delta P_{st-lr}$  the fluids flow from right to the left. According to this argument, at the states that the fluids do not flow (where  $P_4 - P_1 = \Delta P_{st-lr}$ ), the pressure difference can be related to the static contact angle using the Young-Laplace relation as Eqs. 17 and 18:

$$\text{For channel flow: } \Delta P_{st-lr} = \frac{\sigma \cos(\theta_s)}{H} \quad (17)$$

$$\text{For tube flow: } \Delta P_{st-lr} = \frac{2\sigma \cos(\theta_s)}{R} \quad (18)$$

Normally, for the general situations where the fluids are either flowing from left to right or they are stationary, the pressure difference can be written as Eq. 19:

$$P_1 - P_4 = -\Delta P_{st-lr} + \Delta P_D \quad (19)$$

where  $\Delta P_D \geq 0$ . ( $\Delta P_D = 0$  means the fluids do not flow).

Therefore, by substituting Eqs. 17 and 19 in Eq. 13 and Eqs. 18 and 19 in Eq. 14, the Eqs. 20 and 21 are derived:

$$\text{For channel flow: } \cos(\theta_d) - \cos(\theta_s) = \frac{3L}{H} (Ca_2 + Ca_1) - \frac{H\Delta P_D}{\sigma} \quad (20)$$

$$\text{For tube flow: } \cos(\theta_d) - \cos(\theta_s) = \frac{4L}{R} (Ca_2 + Ca_1) - \frac{R\Delta P_D}{2\sigma} \quad (21)$$

For the cases where  $Ca_2 \ll Ca_1$  (e.g., the viscosity of the receding fluid ( $\mu_2$ ) is negligible in comparison with the viscosity of the advancing fluid ( $\mu_1$ )), the equations simplify to Eqs. 22 and 23:

$$\text{For channel flow: } \cos(\theta_d) - \cos(\theta_s) = \frac{3LCa_1}{H} - \frac{H\Delta P_D}{\sigma} \quad (22)$$

$$\text{For tube flow: } \cos(\theta_d) - \cos(\theta_s) = \frac{4LCa_1}{R} - \frac{R\Delta P_D}{2\sigma} \quad (23)$$

And for the cases where  $Ca_1 \ll Ca_2$  (e.g. the viscosity of the advancing fluid ( $\mu_1$ ) is negligible in comparison with the viscosity of the receding fluid ( $\mu_2$ )), the equations are simplified to Eqs. 24 and 25:

$$\text{For channel flow: } \cos(\theta_d) - \cos(\theta_s) = \frac{3LCa_2}{H} - \frac{H\Delta P_D}{\sigma} \quad (24)$$

$$\text{For tube flow: } \cos(\theta_d) - \cos(\theta_s) = \frac{4LCa_2}{R} - \frac{R\Delta P_D}{2\sigma} \quad (25)$$

All the above equations for  $\theta_d$ , make a relation among three unknown parameters of dynamic contact angle, pressure difference, and average velocity. Therefore, another two relations are needed among these three variables to close the system of equations. One additional equation can be the same as the experimental relationships obtained for the dynamic contact angle, some of which were mentioned in the introduction section (e.g., Eqs. 1 and 2). Moreover, almost all

previous researches have considered the conditions in such a way that the pressure at the inlet and outlet of the capillary is the same as the atmospheric pressure and as a result one of the unknowns have also been removed (because  $P_1 - P_4 = 0$ ). Therefore, the system of equations can be solved now with two remained unknowns and two equations.

## Model Validation

Hilpert [24] solved the quasi-steady problem of liquid infiltration into a capillary tube where it was assumed that the initial dynamic contact angle was  $90^\circ$  ( $\theta_{d,0} = 90^\circ$ ),  $L_{l,0} = 0$ ,  $P_1 - P_4 = 0$  and  $\theta_s = 40^\circ$ . Because of the low viscosity of the air (as the receding phase), a single-phase flow was assumed by Hilpert [24]. The same problem was solved numerically by combining Bracke's model (Eq. 2) with Eq. 16 by assuming that  $Ca_2 \ll Ca_1$ . This was because the viscosity of the air is much lower than the liquid.

Fig. 3 compares the results of the obtained dynamic contact angle as a function of dimensionless time ( $\tau = \frac{t\sigma}{\mu R}$ ) between the present work and Hilpert's study [24]. As it is clear, the results are in fair agreement. This approves the validity of the present method. The results obtained by Li et al. [30] were also shown in the same figure.

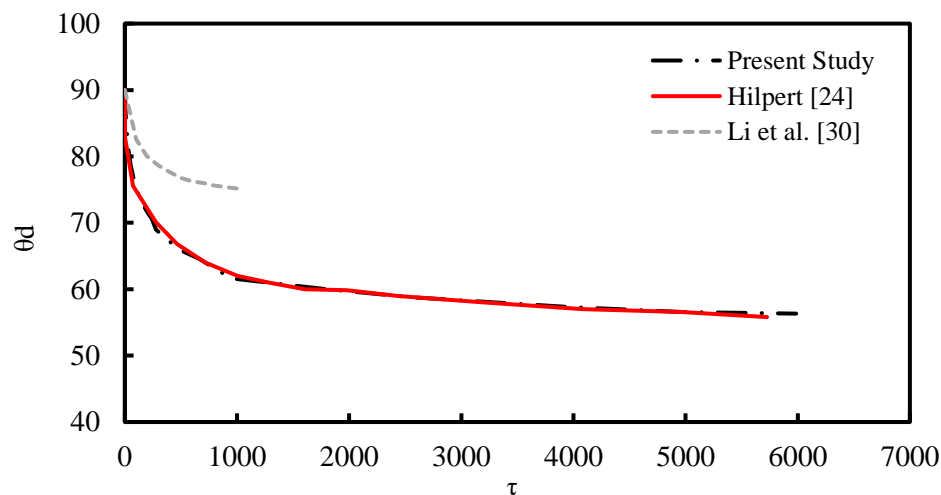


**Fig. 3.** Comparison among the results of the present study for the dynamic contact angle as a function of dimensionless time with the results of Hilpert [24] and Li et al. [30]

By proving the validity of the model, it was used for a variety of situations.

## Results and Discussion

Eqs. 11 and 12 show relations in the most general way for the dynamic contact angles observed in a two-phase flow inside the capillary channel and tube, respectively. According to these equations, the dynamic contact angle is a function of the dimensionless pressure differences between the two ends of the channel/tube, the Capillary numbers of both phases, and the characteristic lengths of the channel/tube. It is necessary to mention that the pressure difference ( $P_1 - P_4$ ), the average velocity ( $\bar{U}$ ) and the contact angle ( $\theta_d$ ) are not independent of each other. Actually, according to these relations, an increase in  $P_1 - P_4$  is compensated by the tolerable decrease in the dynamic contact angle ( $\theta_d$ ) and an increase in the value of the average velocity of the flows ( $\bar{U}$ ). However, the main point is that the instantaneous values of these variables satisfy Eqs. 11 and 12 for the channel and the tube, respectively.

Eqs. 13 and 14 express the same relations for the steady flows, and Eqs. 15 and 16 do the same for the time-dependent flows. Eqs. 20 and 21 provide a clearer picture of the relationship between the dynamic ( $\theta_d$ ) and the static ( $\theta_s$ ) contact angles. Eqs. 22 to 25 simplify the mentioned relations for the special cases where the Capillary number of one of the fluids is much lower than the other.

Showing the results obtained by these equations in graphical format is useful. Therefore, in following, the effects of viscosity ratio and length to radius ratio on the dynamic contact angle will be discussed.

### Effect of Viscosity Ratio

Unlike the single-phase flows, no experimental relation has been provided so far to predict the dynamic contact angle in two-phase flows with comparable viscosities. Therefore, solving Eqs. 11 and 12 is not possible in its general form because of the smaller number of equations (equal to 1) than the variables (equal to 3). However, it is possible to reduce the variables by investigating a simpler case where  $P_1 - P_4 = 0$ . For such a case still two unknowns ( $\theta_d$  and  $\bar{U}$ ) exist. As a simple first-order estimation, it is possible to assume that Bracke's model (Eq.2) is still usable. However, Bracke's model is dedicated to the tube flows. Therefore, only Eq. 12 was solved numerically for such a case, and the results are shown in Figs. 4 to 8.

In Figs. 4 to 6, the evolution of the dynamic contact angle inside a tube is shown versus dimensionless time at different values of viscosity ratios of the phases ( $\mu_1/\mu_2$ ) for initial values of,  $\theta_{d,0} = 90^\circ, 75^\circ, 60^\circ$  respectively. The static contact angle ( $\theta_s$ ) was equal to  $40^\circ$  for all these cases. As it is clear, with increasing in viscosity ratio ( $\mu_1/\mu_2$ ), the evolution of the contact angle with dimensionless time become faster. In fact, when the first fluid does not change (means constant values of  $\mu_1$ ) while the second fluid becomes less viscous, the dynamic contact angle changes occur faster to reach the final value. This is because the resistance against the flow in the second phase decreases by the decrease of  $\mu_2$ .

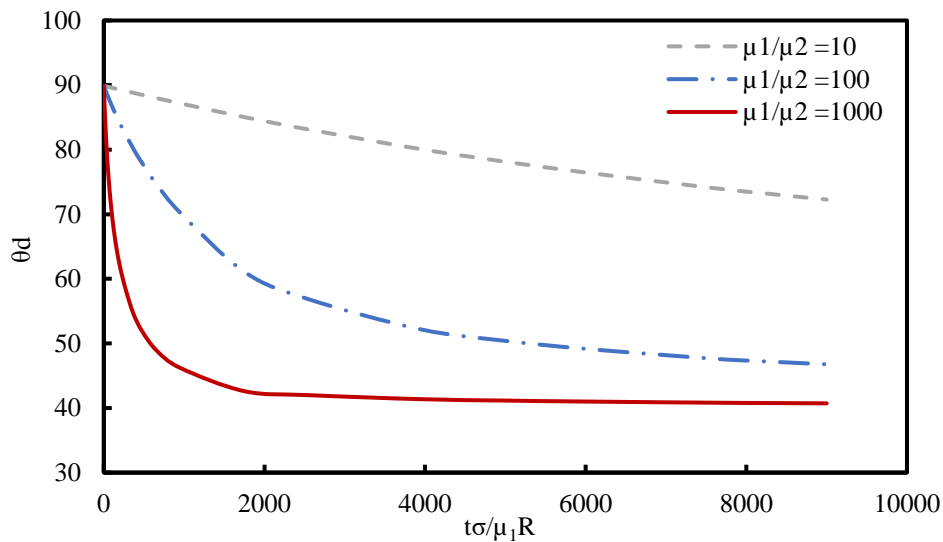


**Fig. 4.** Dynamic contact angle in a tube as a function of dimensionless time for different values of  $\mu_1/\mu_2$  for a case with an initial dynamic contact angle of  $90^\circ$

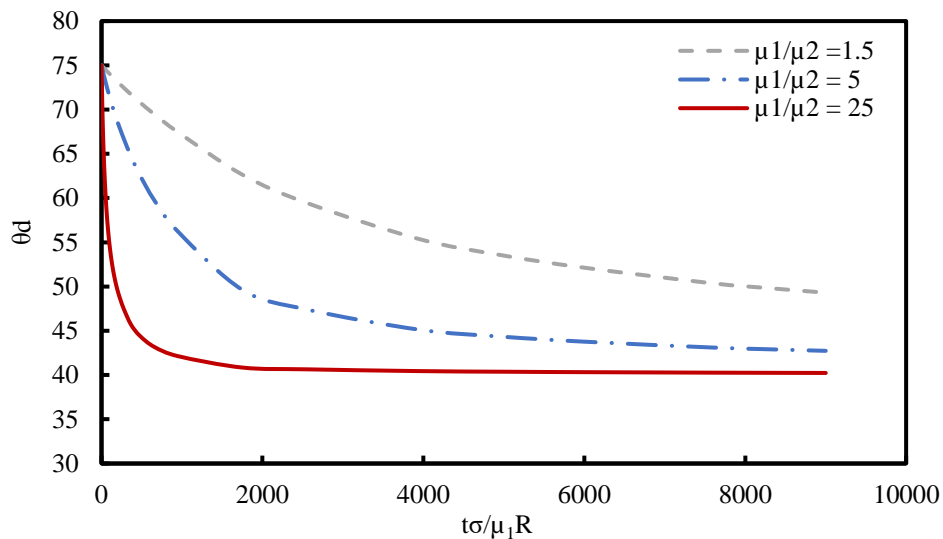


**Fig. 5.** Dynamic contact angle in a tube as a function of dimensionless time for different values of  $\mu_1/\mu_2$  for a case with an initial dynamic contact angle of  $75^\circ$

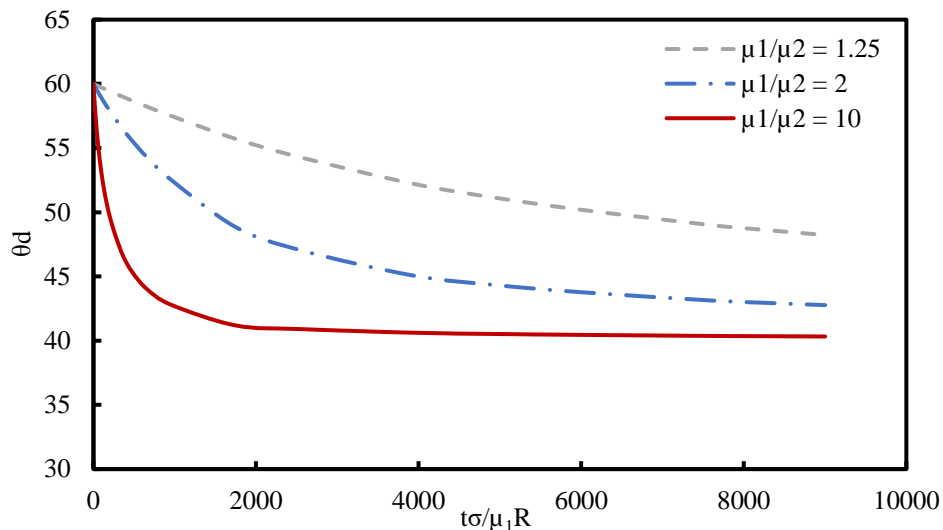


**Fig. 6.** Dynamic contact angle in a tube as a function of dimensionless time for different values of  $\mu_1/\mu_2$  for a case with an initial dynamic contact angle of  $60^\circ$

For all those cases shown in Figs. 4 to 6, the time was dimensionless by the value of  $\mu_1$  as a constant parameter. However, the time can become dimensionless by using  $\mu_2$  (as a changing parameter) instead of  $\mu_1$ . Fig. 7 shows such data for a case of initial dynamic contact angle of  $90^\circ$  and static contact angle of  $40^\circ$ . Comparing Fig. 7 with Fig. 4, the graphs with different values of  $\mu_1/\mu_2$  are superimposed, and the differences are faded. This indicates that although by keeping  $\mu_1$  constant and  $\mu_2$  decreasing, the real time of equilibrium decreases, these differences, if examined in the context of dimensionless time by the changing factor (here  $\mu_2$ ) will disappear. A master curve is obtained that summarizes all the data. Other master curves can also be achieved for the data shown in Figs. 5 and 6.

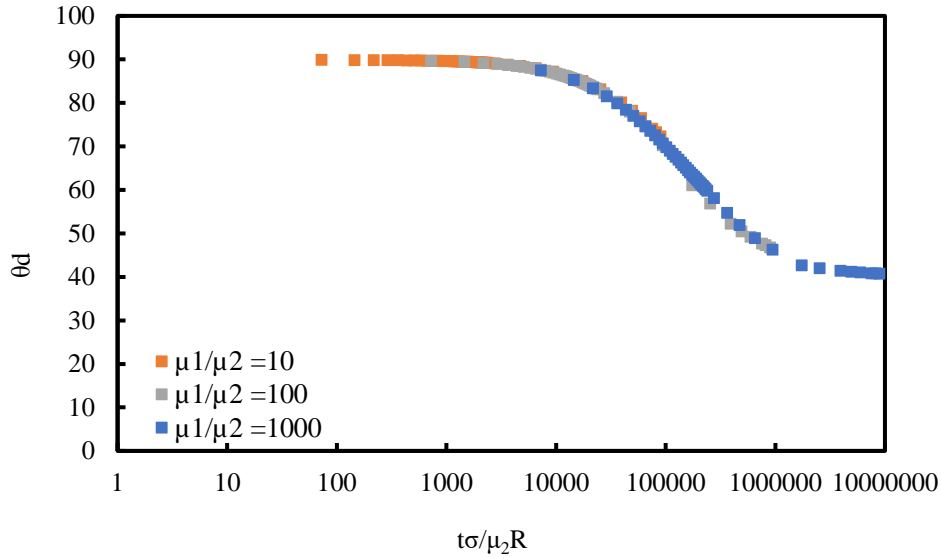


**Fig. 7.** Dynamic contact angle in a tube when the time has become dimensionless with the changing parameter (here  $\mu_2$ )

### Effect of Length Ratio

Characteristic lengths are also effective parameters on the dynamic contact angle according to Eqs. 11 and 12. Fig. 8 shows the effect of the ratio of length to the diameter of the tube ( $L/R$ ) on the evolution of the dynamic contact angle for a case with  $\theta_{d,0} = 90^\circ$  and  $\mu_1/\mu_2 = 100$ . According to this figure, increasing the value of  $L/R$  leads to a slower process of reduction of the contact angle with time. Actually, for the tubes with larger  $L/R$  ratios, the contact angle has more time to change from its initial value to its final value.

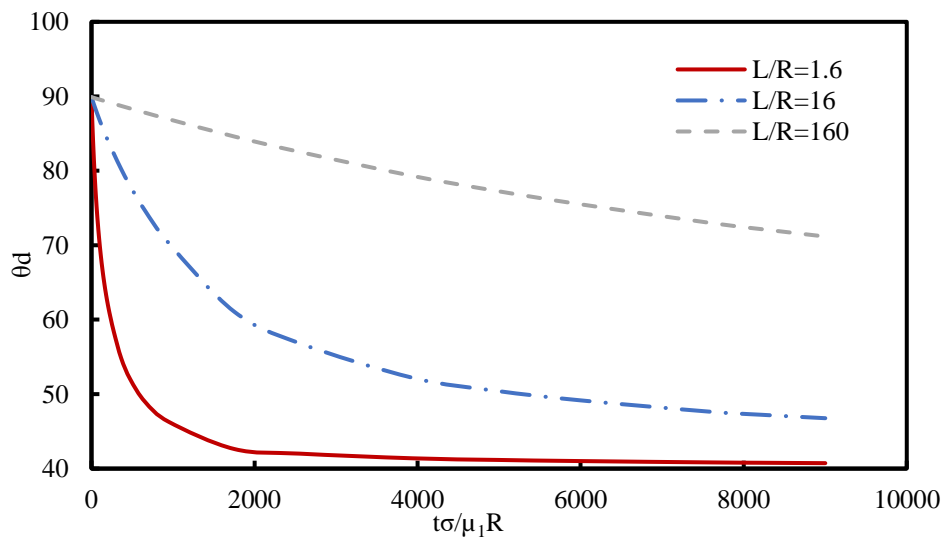


**Fig. 8.** Dynamic contact angle in a tube as a function of dimensionless time for different values of  $L/R$  for a case with initial dynamic contact angle of  $90^\circ$

The same data are shown in Fig.9, but the time became dimensionless by the tube's length ( $L$ ) rather than its radius ( $R$ ). Again a master curve is observed. It is needed to notice that  $L$  was the changing parameter in all the graphs.

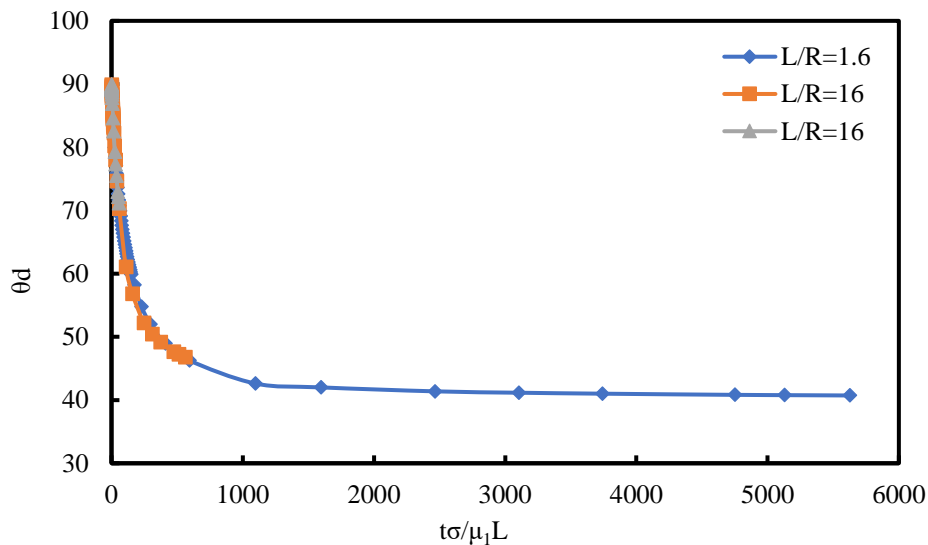


**Fig. 9.** Dynamic contact angle in a tube when the time has become dimensionless with the changing parameter (here  $L$ )

According to Figs. 7 and 9, it can be claimed that a master curve and a unique behavior is expected for the evolution of the dynamic contact with the dimensionless time if the time was become dimensionless by the changing parameter.

## Conclusion

In the present study, using a simplified mathematical model based on the Navier-Stokes equations, along with the Young-Laplace equation, the problem of quasi-steady motion of the contact line between two immiscible fluids within a capillary channel and a capillary tube was solved. For this model, several common assumptions, including Newtonian fluid, incompressible, laminar, and fully developed flow were assumed. In addition, the quasi-steady-state condition and linear pressure drop for each fluid along the channel/tube were assumed. The effect of gravity was also ignored due to the low Bond number.

Based on the model predictions, it was found that the dynamic contact angle observed in a two-phase flow has a direct relation with the dimensionless pressure difference between the two ends of the channel/tube, the Capillary numbers of both phases and the ratio of the geometric characteristic lengths of the channel ( $L/H$ ) and of the tube ( $L/R$ ). The effects of these parameters, although some of them were previously qualitatively proven, were never explicitly expressed quantitatively before. It was also useful to divide the dimensionless pressure difference to the two terms of the static contact angle and the remaining pressure. This clarifies the role of the static contact angle in determining the dynamic contact angle.

The model was validated by comparing its results for the dynamic contact angle versus dimensionless time for a case of water-air flow with the literature data. After validation, it was applied for situations with different viscosity ratios ( $\mu_1/\mu_2$ ) and different characteristic length ratios ( $L/R$ ). It was found that the evolution of the dynamic contact angle (from the initial value to the equilibrium value) slows down with decreasing in  $\mu_1/\mu_2$  and vice versa. However, it was found that if the time becomes dimensionless with the changing parameter (here  $\mu_2$ ), a master curve is obtained that holds all the data together. Also, it was seen that with increasing the value of the ratio of the length to the radius of the tube ( $L/R$ ), the evolution of the dynamic contact

angle slows down. Again, a master curve was obtained when the time was become dimensionless by the changing parameter (here  $L$ ). Finding master curves facilitates predicting and interpreting the dynamic contact angle results that may be obtained in a variety of experimental or modeling ways.

The presented model proves that in a two-phase flow inside a confined media (*e.g.*, a tube or channel), the changes in the time context of the dynamic contact angle are not only influenced by the properties (*e.g.* viscosity or  $Ca$  number) of the advancing phase but also by the properties of the preceding phase. Moreover, the characteristic length ratios are also effective parameters for the evolution of the dynamic contact angle. These findings, although came from a simplified model and a first-order solution, make new insights into the understanding of the evolution of the dynamic contact angle in two-phase microscale flows.

## Nomenclature

$Bo$	Bond number
$Ca$	Capillary number
$Ca_1$	Capillary number of fluid 1
$Ca_2$	Capillary number of fluid 2
$H$	Half the width of the channel
$L_1$	Channel/tube length of the left side
$L_{1,0}$	Initial value of $L_1$
$L_2$	Channel/tube length of the right side
$L_{2,0}$	Initial value of $L_2$
$P_1$	Pressure at the inlet
$P_2$	Pressure at the left side of the interface
$P_3$	Pressure at the right side of the interface
$P_4$	Pressure at the outlet
$R$	Radius of the tube
$r$	Radial coordinate
$S$	Microscopic length
$y$	Y-component of Cartesian coordinate
$t$	Time
$\bar{U}$	Average velocity of the fluid
$u_1$	Velocity of fluid 1
$u_2$	Velocity of fluid 2
$g$	Gravity acceleration
$\beta$	A constant in Eq. 4
$\Delta P_{st-lr}$	Pressure difference at which fluids do not flow
$\Delta P_D$	Remaining pressure difference
$\theta_d$	Dynamic contact angle
$\theta_{d,0}$	Initial value of dynamic contact angle
$\theta_s$	Static contact angle
$\mu_1$	Viscosity of fluid 1
$\mu_2$	Viscosity of fluid 2
$\sigma$	Surface tension coefficient

## References

- [1] Prokopev S, Vorobev A, Lyubimova T. Phase-field modeling of an immiscible liquid-liquid displacement in a capillary. *Physical Review E*. 2019;99(3):033113.
- [2] Wu P, Nikolov AD, Wasan DT. Capillary rise: validity of the dynamic contact angle models. *Langmuir*. 2017;33(32):7862-72.
- [3] Liu J, Sheng JJ, Wang X, Ge H, Yao E. Experimental study of wettability alteration and spontaneous imbibition in Chinese shale oil reservoirs using anionic and nonionic surfactants. *Journal of Petroleum Science and Engineering*. 2019;175:624-33.
- [4] Blake T, Batts G. The temperature-dependence of the dynamic contact angle. *Journal of colloid and interface science*. 2019;553:108-16.
- [5] Wang X, Min Q, Zhang Z, Duan Y, Zhang Y, Zhai J. Influence of head resistance force and viscous friction on dynamic contact angle measurement in Wilhelmy plate method. *Colloids and Surfaces A: Physicochemical and Engineering Aspects*. 2017;527:115-22.
- [6] Burley R, Jolly RP. Entrainment of air into liquids by a high speed continuous solid surface. *Chemical Engineering Science*. 1984;39(9):1357-72.
- [7] Hoffman RL. A study of the advancing interface. I. Interface shape in liquid—gas systems. *Journal of colloid and interface science*. 1975;50(2):228-41.
- [8] Wilson S. A note on the measurement of dynamic contact angles. *Journal of Colloid and Interface Science*. 1975;51(3):532-4.
- [9] Thompson PA, Robbins MO. Simulations of contact-line motion: slip and the dynamic contact angle. *Physical Review Letters*. 1989;63(7):766.
- [10] Omori T, Kajishima T. Apparent and microscopic dynamic contact angles in confined flows. *Physics of Fluids*. 2017;29(11):112107.
- [11] Eggers J, Stone HA. Characteristic lengths at moving contact lines for a perfectly wetting fluid: the influence of speed on the dynamic contact angle. *Journal of Fluid Mechanics*. 2004;505:309-21.
- [12] Šikalo Š, Wilhelm H-D, Roisman I, Jakirlić S, Tropea C. Dynamic contact angle of spreading droplets: Experiments and simulations. *Physics of Fluids*. 2005;17(6):062103.
- [13] Jiang T-S, Soo-Gun O, Slattery JC. Correlation for dynamic contact angle. *Journal of colloid and interface science*. 1979;69(1):74-7.
- [14] Bracke M, De Voeght F, Joos P. The kinetics of wetting: the dynamic contact angle. *Trends in Colloid and Interface Science III*: Springer; 1989. p. 142-9.
- [15] Kamyabi A, SA AR, Kamyabi M. Surfactant effects on the efficiency of oil sweeping from the dead ends: Numerical simulation and experimental investigation. *Chemical Engineering Research and Design*. 2015;94:173-81.
- [16] De Gennes P-G. Wetting: statics and dynamics. *Reviews of modern physics*. 1985;57(3):827.
- [17] Cox R. The dynamics of the spreading of liquids on a solid surface. Part 1. Viscous flow. *Journal of fluid mechanics*. 1986;168:169-94.
- [18] Hocking L. A moving fluid interface. Part 2. The removal of the force singularity by a slip flow. *Journal of Fluid Mechanics*. 1977;79(2):209-29.
- [19] Blake TD. The physics of moving wetting lines. *Journal of colloid and interface science*. 2006;299(1):1-13.
- [20] De Ruijter MJ, Blake T, De Coninck J. Dynamic wetting studied by molecular modeling simulations of droplet spreading. *Langmuir*. 1999;15(22):7836-47.
- [21] Rolley E, Guthmann C. Dynamics and hysteresis of the contact line between liquid hydrogen and cesium substrates. *Physical review letters*. 2007;98(16):166105.
- [22] Fermigier M, Jenffer P. An experimental investigation of the dynamic contact angle in liquid-liquid systems. *Journal of colloid and interface science*. 1991;146(1):226-41.
- [23] Washburn EW. The dynamics of capillary flow. *Physical review*. 1921;17(3):273.
- [24] Hilpert M. Effects of dynamic contact angle on liquid infiltration into horizontal capillary tubes:(Semi)-analytical solutions. *Journal of colloid and interface science*. 2009;337(1):131-7.
- [25] Hilpert M. Effects of dynamic contact angle on liquid withdrawal from capillary tubes:(Semi)-analytical solutions. *Journal of colloid and interface science*. 2010;347(2):315-23.
- [26] Hilpert M. Explicit analytical solutions for liquid infiltration into capillary tubes: Dynamic and constant contact angle. *Journal of colloid and interface science*. 2010;344(1):198-208.



- [27] Hilpert M. Liquid withdrawal from capillary tubes: explicit and implicit analytical solution for constant and dynamic contact angle. *Journal of colloid and interface science*. 2010;351(1):267-76.
- [28] Cai J, Perfect E, Cheng C-L, Hu X. Generalized modeling of spontaneous imbibition based on Hagen–Poiseuille flow in tortuous capillaries with variably shaped apertures. *Langmuir*. 2014;30(18):5142-51.
- [29] Cai J, Hu X, Standnes DC, You L. An analytical model for spontaneous imbibition in fractal porous media including gravity. *Colloids and Surfaces A: Physicochemical and Engineering Aspects*. 2012;414:228-33.
- [30] Li C, Shen Y, Ge H, Zhang Y, Liu T. Spontaneous imbibition in fractal tortuous micro-nano pores considering dynamic contact angle and slip effect: phase portrait analysis and analytical solutions. *Scientific reports*. 2018;8(1):1-13.

**How to cite:** Kamyabi M, Kamyabi A. On the Dynamic Contact Angle in Capillary Flows. *Journal of Chemical and Petroleum Engineering*. 2021; 55(2): 243-256.